Quantifying uncertainties in direct-numerical-simulation statistics due to wall-normal numerics and grids

Peng E. S. Chen, Xiaowei Zhu, Yipeng Shi, and Xiang I. A. Yang

Phys. Rev. Fluids **8**, 074602 — Published 10 July 2023

DOI: 10.1103/PhysRevFluids.8.074602

Quantifying uncertainties in DNS statistics due to wall-normal numerics and grids

Peng E S Chen,[1,2], Xiaowei Zhu[3], Yipeng Shi[1,2], and Xiang I A Yang[4a]
[1]College of Engineering, Peking University, China, 100871
[2]State Key Laboratory of Turbulence and Complex Systems, Beijing, China, 100871
[3]Department of Mechanical and Materials Engineering, Portland State University, OR, USA, 97207
[4]Mechanical Engineering, Pennsylvania State University, PA, USA, 16802

This paper takes the perspective of a user of DNS data and quantifies the uncertainties in DNS statistics for plane channel flows. We focus on high-order statistics, such as skewness, kurtosis, and viscous dissipation, and quantify the uncertainties due to wall-normal numerics and grids while minimizing the sampling error and the discretization error in the wall-parallel directions. Two grid distributions and four discretization methods are considered, which are representative of the existing DNSs. Our results show that the available DNS data contain at least a 7% uncertainty in the computed mean viscous dissipation in the buffer layer. Moreover, since turbulence becomes more intermittent at higher Reynolds numbers, the flow will be less well-resolved at the higher Reynolds number if the same grid resolution in terms of the viscous units is employed. Specifically, our estimate shows that a grid that resolves 90% of the dissipation events at $Re_\tau = 544$ resolves about 87% of the dissipation events at $Re_\tau = 10000$.

I. INTRODUCTION

Plane channel flow is a simple type of wall-bounded flow that occurs between two infinitely large parallel planes. Over the last few decades, channel flows have been widely studied, and direct numerical simulation (DNS) of channel flows has become increasingly common among researchers. The first DNS of channel flow was performed in the 1980s by Kim et al. [1], at a friction Reynolds number of $Re_\tau = 180$. Since then, researchers have conducted numerous DNS studies, with the most recent one performed by Hoyas and Oberlack [2] at a friction Reynolds number of $Re_\tau = 10000$. These high-fidelity DNS data are often regarded as truth and have served as references for numerous theoretical studies [3];

Consider, for example, the recent discussion on the Reynolds number scaling of the dissipation rate. Yang and Lozano-Duran [4] argued that the dissipation rate at the wall should scale as $\epsilon^+_{w,x} \sim C_1 \ln(Re_\tau) + C_2$, where ϵ_x is the dissipation due to the shear in the streamwise direction, Re_τ is the friction Reynolds number, the subscript w denotes wall quantities, C_1 and C_2 are two constants. Chen and co-authors [5, 6], on the other hand, argued that the dissipation at the wall should scale as $\epsilon^+_{w,x} \sim C_1' - C_2' Re_\tau^{-1/4}$, where C_1' and C_2' are two constants. The two scalings give distinctly different scaling estimates at infinite Reynolds numbers. The scaling in Ref. [4] predicts that the dissipation rate increases indefinitely with the Reynolds number, while the scaling in Ref. [6] predicts that it is finite. Nonetheless, the two scalings give similar estimates at $Re_\tau \lesssim O(10^5)$. Specifically, the scaling in Ref. [4] gives 0.213 at $Re_\tau = 30000$, and the scaling in Ref. [7] gives 0.218, and the difference is only 2%. DNS data for channel flows have been instrumental in determining the scaling of the dissipation rate. However, to confirm one scaling and refute the other, the uncertainty in the data must be less than 2%. The above discussion applies equally to the scalings in Refs. [8, 9]. To that end, understanding the underlying uncertainties of DNS data is crucial.

Many studies have estimated the uncertainties in channel flow DNSs [10–12]. The expected error is less than 1% and 3% in the mean flow and the velocity root-mean-square (RMS), respectively, if one employs the "typical" grid resolution and sampling time at $Re_\tau = 180$. The typical grid resolution is determined based on heuristics established in Refs. [7, 10, 13]. According to these heuristics, the grid spacing in the streamwise and the spanwise directions should be $\Delta x^+ \approx 10$ and $\Delta z^+ \approx 5$. For pseudo-spectral codes, slightly coarser grids may be adequate, while finite difference codes may require slightly finer grids [14]. The grid spacing in

[a] Email: xzy48@psu.edu

the wall-normal direction is less straightforward. Historically, Δy was scaled with the wall unit [15]. Yang et al. [16] and Pirozzoli and Orlandi [17] recently pointed out that $\Delta y^+ \approx 6$ leads to excessive grid resolution at the channel center, especially at high Reynolds numbers. Following the arguments in Refs. [16, 17], the wall-normal grid spacing should resolve the wall unit in the viscous layer and the local Kolmogorov length scale in the logarithmic and the wake layers, respectively. The heuristics for the sampling time, on the other hand, suggest that $10\delta/u_\tau$ is needed to obtain converged first- and second-order statistics, although shorter (and sometimes much shorter) sampling time is often used [18].

The above heuristics have been challenged in the recent literature, particularly at high Reynolds numbers. Donzis et al. [19] argued that since turbulence becomes more intermittent as the Reynolds number increases, one must employ finer grids at higher Reynolds numbers to resolve the flow as well as at a low Reynolds number. Following the arguments in Ref. [19], Yakhot et al. [20] estimated the grid resolution needed in order to resolve a given order moment of velocity derivatives in isotropic turbulence, and Yang et al. [21] estimated the horizontal grid resolution needed to resolve 99% of the wall-shear stress events in a plane channel. In this context, the following question remains open: What are the uncertainties in high-order statistics like dissipation, velocity skewness, and kurtosis? Notice that the wording here is "uncertainty" rather than "error". Here, we take a user's perspective: For someone who uses DNS data for theoretical analysis, differences between DNS datasets are more often than not viewed as uncertainties rather than errors.

This work aims to answer the above question. We will quantify the uncertainties due to the discretization in the wall-normal direction by considering grid distributions and discretizations that are representative of the existing DNSs, namely, cosine and naturally stretched girds [17], Chebyshev [1, 12, 22–24], 2nd-order finite difference [14, 25, 26], 3rd- and 7th-order B-spline [27, 28] discretizations. Again, the objective here is to quantify the uncertainty rather than provide guidelines for DNS practitioners. We will not make judgments about discretization methods or grid distributions.

The remainder of the paper is organized as follows. We present the DNS setup in Sect. II. The results are shown in Sect. III, followed by conclusions in Sect. IV.

II. DNS DETAILS

We solve the incompressible Navier-Stokes equation in a periodic plane channel. The flow is driven by a constant pressure gradient. The grids are uniform in the streamwise and spanwise directions, respectively. The wall-normal grids are stretched according to either a cosine function [1]

$$\frac{y_j}{\delta} = \cos\left(\frac{j}{N_y - 1}\pi\right), \tag{1}$$

or the following natural stretching function [17]

$$y_j^+ = \frac{1}{1 + (j/j_b)^2}\left[\Delta y_w^+ j + \left(\frac{3}{4}\alpha c_\eta j\right)^{4/3}(j/j_b)^2\right]. \tag{2}$$

Differentiating Eqs. (1) and (2) gives the grid spacing:

$$\frac{\Delta y_j}{\delta} = -\frac{1}{\delta}\frac{dy_j}{dj} = \frac{\pi}{N_y - 1}\sin\left(\frac{j}{N_y - 1}\pi\right), \tag{3}$$

and

$$\Delta y_j^+ = \frac{dy_j^+}{dj} = \frac{1}{\left(1 + (j/j_b)^2\right)^2}\left[\left(1 - \left(\frac{j}{j_b}\right)^2\right)\Delta y_w^+ + \frac{2}{3}\left(\frac{3}{4}\alpha c_\eta\right)^{\frac{4}{3}}\frac{j^{\frac{7}{3}}}{j_b^2}\left(5 + 2\left(\frac{j}{j_b}\right)^2\right)\right]. \tag{4}$$

Here, $j = 0,\ 2,\ \ldots\ ,\ N_y - 1$ in Eqs. (1) and (3), and $j = 0,\ 2,\ \ldots\ ,\ N_y/2 - 1$ in Eqs. (2) and (4), N_y is the

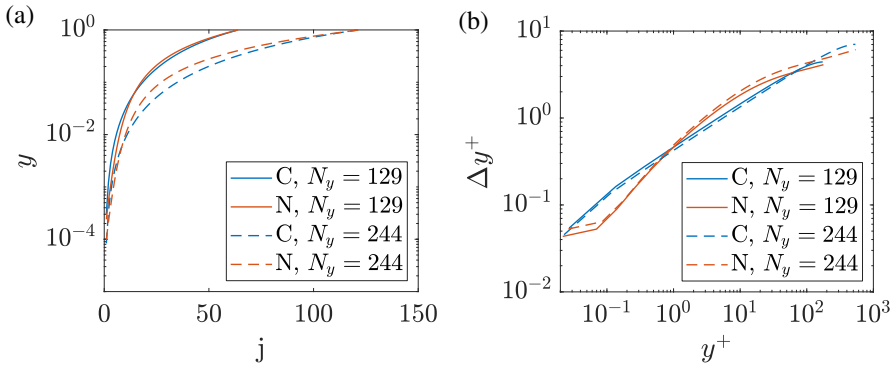

FIG. 1. (a) Grid distribution. (b) Distribution of the grid spacing. Here, C stands for cosine, i.e., Eq. (1), and N stands for natural stretching, i.e., Eq. (2).

number of grid points in the wall-normal direction; α in Eq. (2) controls the grid resolution at the center of the channel, i.e., $\Delta y^+ = \alpha\eta^+$, $\eta = \left(\nu^3/\epsilon\right)^{1/4}$ is the local Kolmogorov scale, and $\alpha = 1.5$ [17]; $c_\eta = 0.8$ is a constant; $j_b = 16$ controls the number of grid points in the wall layer (viscous sublayer and the buffer layer); $\Delta y_w^+ = 0.05$ is the grid resolution at the wall. Equation (1) leads to excessive grids in the wall-normal direction at high Reynolds numbers. To resolve this issue, Lee and Moser, among others [27, 28], proposed the following wall-normal grid

$$\frac{y}{\delta} = \frac{\sin(\beta\xi\pi/2)}{\sin(\beta\pi/2)}, \quad \xi = \frac{2j}{N_y - 1} - 1, \tag{5}$$

where $\beta \leq 1$ controls the grid clustering in the wall layer. Lee and Moser took $\beta = 0.97$ for the $Re_\tau = 5200$ DNS and $\beta \approx 1$ for the DNSs at $Re_\tau = 180$ and 544 [27]. The DNSs in this work are at the Reynolds numbers $Re_\tau = 180$, 544. We follow Ref. [27] and take $\beta = 1$.

Figure 1 shows the distribution of the grid, i.e., y_j as a function of j, and the distribution of the wall-normal grid spacing, i.e., $\Delta y_j = y_{j+1} - y_j$ as a function of y_j, for $N_y = 129$ and 244. Here, the $N_y = 129$ grid is intended for a $Re_\tau = 180$ channel, and the $N_y = 244$ grid is intended for a $Re_\tau = 544$ channel. We use the same number of grid points to compare their grid spacing on a similar cost basis. Equation (2) gives rise to a quick increase in Δy^+ from the 2nd off-wall grid to the 3rd off-wall grid, as shown in figure 1 (b) (see also figure 5b in Ref. [17]). At these Reynolds numbers, the cosine stretching does not lead to undesirable grid clustering at the wall. We see from figure 1 that the natural stretching gives slightly higher resolutions at the first few off-wall grid points and the channel centerline but slightly lower resolutions in the buffer layer and the logarithmic layer than the cosine stretching.

Three codes are employed, namely, the code in Ref. [1], the code in Ref. [27], and the code in Ref. [29–31]. The three codes use the same spectral method in the wall-parallel directions. Discretization in the wall-normal direction is via the Chebyshev spectral method (SP), the B-spline method (BS), and the finite difference method (FD), respectively. The B-spline method is either third order or seventh order, which is referred to as BS3 or BS7. The finite difference method is second order, referred to as FD2. Note that the Chebyshev spectral method is compatible with the cosine grid only. Further details of the three codes are shown in Table I.

Table II shows the details of the DNSs, including the Reynolds number, the averaging time, the grid size, and the resolution in plus units. Two Reynolds numbers are considered, i.e., $Re_\tau = 180$ and 544 (nominal Reynolds number, computed according to $Re_\tau = \delta\sqrt{-1/\rho\ dP/dx}\ \delta/\nu$). The size of the computational domain is $L_x \times L_y \times L_z = 4\pi\delta \times 2\delta \times 2\pi\delta$. The grid spacings in the streamwise and the spanwise directions are such that they resolve more than 99% of the dissipation (wall-shear stress) events at the wall [21], which, as we will see, is sufficient for the purpose of the current study. The number of grid points is such that $\Delta y_w^+ \approx 0.05$ for the cosine stretched grid and $y_{N_y}^+$ computed according to Eq. (2) just exceeds Re_τ. This leads to a slightly different number of grid points when a grid is stretched according to the cosine function

TABLE I. Details of the codes. Here, "disc." is short for discretization, "conv." is short for convective, "visc." is short for viscous, "AB" is short for Adam-Bashforth, "RK" is short for Runge-Kutta, and "C-N" is short for Crank-Nicolson.

Code	x, z disc.	y disc.	Time disc.	
			conv. terms	visc. terms
SP	Fourier spectral	Chebyshev	2nd AB	C-N
BS7	Fourier spectral	7th B-spline	3rd RK	C-N
BS3	Fourier spectral	3rd B-spline	3rd RK	C-N
FD2	Fourier spectral	2nd finite difference	2nd AB	C-N

TABLE II. DNS details. $Re_\tau = u_\tau \delta/\nu$ is the computed friction Reynolds number, which only equals the nominal friction Reynolds number if the averaging time approaches infinity. T_r is the averaging time. D_x^+ and D_z^+ are the grid spacings in the streamwise and the spanwise directions. $D_{y,w}^+$ and $D_{y,c}^+$ are the wall-normal grid spacing at the wall and the center of the channel. The nomenclature of the cases is as follows: [Code][Grid]R[Re_τ], where [Code] is SP, BS3, BS7, or FD2, [Grid] is C (cosine), CF (fine grid, cosine), or NS (natural stretching), [Re_τ] is 180 or 544.

Case	Re_τ	$T_r u_\tau/\delta$	$N_x \times N_y \times N_z$	$D_x^+ \times (D_{y,w}^+, D_{y,c}^+) \times D_z^+$
SPCR180	181.41	32	$192 \times 130 \times 180$	$11.7 \times (0.054, 4.42) \times 6.26$
SPCFR180	180.27	32	$192 \times 259 \times 180$	$11,7 \times (0.013, 2.19) \times 6.22$
BS7CR180	182.29	32	$192 \times 129 \times 180$	$12.0 \times (0.055, 4.48) \times 6.37$
BS3CR180	182.02	32	$192 \times 133 \times 180$	$12.0 \times (0.052, 4.33) \times 6.37$
BS3CFR180	182.23	32	$192 \times 259 \times 180$	$12.0 \times (0.014, 2.22) \times 6.37$
FD2CR180	180.70	32	$192 \times 129 \times 180$	$11.8 \times (0.053, 4.38) \times 6.28$
FD2NR180	179.30	32	$192 \times 116 \times 180$	$11.8 \times (0.050, 4.59) \times 6.28$
SPCR544	544.95	12	$576 \times 244 \times 540$	$11.8 \times (0.045, 7.01) \times 6.31$
SPCFR544	545.36	12	$576 \times 487 \times 540$	$11.9 \times (0.011, 3.53) \times 6.35$
BS7CR544	543.16	12	$576 \times 237 \times 540$	$11.8 \times (0.048, 7.23) \times 6.32$
BS3CR544	544.72	12	$576 \times 241 \times 540$	$11.9 \times (0.047, 7.13) \times 6.34$
BS3CFR544	544.80	12	$576 \times 484 \times 540$	$11.9 \times (0.012, 3.54) \times 6.34$
FD2CR544	546.04	12	$576 \times 243 \times 540$	$11.8 \times (0.046, 7.06) \times 6.31$
FD2NR544	542.50	12	$576 \times 260 \times 540$	$11.8 \times (0.048, 5.70) \times 6.31$

and the natural stretching function. Table III lists the setups of previous DNSs for comparison purposes. Clearly, our DNSs are representative of the ones in the present literature.

The nomenclature of the DNS cases is as follows: [Code][Grid]R[Re_τ], where [Code] is SP, BS3, BS7, or FD2, [Grid] is C (cosine), CF (fine grid, cosine), or N (natural stretching), [Re_τ] is 180 or 544. We take cases SPCR180 and SPCR544 as our baselines. The SPCFR and the BS3CFR cases use twice as many grid points in the wall-normal direction as the two baseline cases. The same cosine stretched wall-normal grid is used in SPC, BS7C, BS3C, and FD2C.

For this study, the same code is used for the FD2N and FD2C cases. For the $Re_\tau = 180$ and 544 channel flows, the naturally stretched grid is not more cost-effective than the cosine stretched grid, with the cost of FD2NR180 and FD2NR544 1.2 and 1.1 times the cost of FD2CR180 and FD2CR544 (in terms of the wall time). However, since the cosine grid leads to excessive grid clustering at high Reynolds numbers, the natural stretching method will be more cost-effective at high Reynolds numbers.

Before we proceed, we follow the previous authors and check the statistical convergence of our DNSs. We average for $T_r = 32\delta/u_\tau$ and $12\delta/u_\tau$ for the $Re_\tau = 180$ and 544 cases, respectively. The sampling time is comparable to and, in many cases, longer than those in the literature, as we can see in Table III. (Lozano-Duran and Jimenez [24] used a slightly longer averaging time for their $Re_\tau = 950$ and 4200 channel, but their domain size is twice as small.) The present sampling time T_r gives rise to a 1% convergence error in Re_τ. Figure 2 (a, b) show the time history of the normalized instantaneous friction Reynolds number for

TABLE III. A (not comprehensive) survey of channel flow DNSs in the literature. The reference, the friction Reynolds number, the discretization in the three Cartesian directions, the wall-normal grid, and the sampling time are tabulated. Δy_w^+ and Δy_c^+ are the wall-normal grid spacing at the wall and the centerline, respectively. "$\sim \eta$" indicates that the wall-normal grid spacing is proportional to the local Kolmogorov scale $\eta = \left(\nu^3/\epsilon\right)^{1/4}$. We put N/A if the information is not available. "disc." is short for discretization, and "FD" is short for the finite difference. Cosine grid corresponds to Eq. (1). Sine grid corresponds to Eq. (5).

Ref.	$Re_{\tau,\max}$	x, z disc.	y disc.	y grid	Δy_w^+	Δy_c^+	Tu_τ/δ
[1]	180	Fourier	Chebyshev	Cosine	0.05	4.4	10
[12]	392	Fourier	Chebyshev	Cosine	0.05	6.41	10
[22]	590	Fourier	Chebyshev	Cosine	0.04	7.2	N/A
[23]	934	Fourier	Chebyshev	Cosine	0.03	7.6	N/A
[26]	1020	4th FD	2nd FD	N/A	0.15	7.32	6.3
[34]	2003	Fourier	7th CFD	$\sim \eta$	N/A	8.9	11
[24]	932	Fourier	Chebyshev	Cosine	0.03	7.7	20
[24]	4179	Fourier	7th CFD	N/A	N/A	10.7	15
[14]	4079	2nd FD	2nd FD	Cosine	0.02	6.38	8.5
[27]	5186	Fourier	7th B-spline	Sine	0.50	10.3	7.8
[25]	8016	10th FD	2nd FD	$\sim \eta$	0.6	8.0	6.3

cases SPCR180 and SPCR544. It should be clear that the flow is statistically stationary. Figure 3 (a, b) show the terms in the following Reynolds averaged momentum equation:

$$-\langle u'v'\rangle^+ + \left(\frac{dU}{dy}\right)^+ = 1 - \frac{y}{\delta} \tag{6}$$

where $-\langle u'v'\rangle$ is the Reynolds shear stress, U is the mean velocity. If the flow is statistically converged, the sum of the turbulent and viscous flux is a linear function of y, which is often invoked to check the statistical convergence of a channel flow simulation [7, 10, 13, 25, 27, 32, 33]. Figure 3 shows the terms in the mean momentum equation in cases SPCR180 and SPCR544. We see that the sum of the two fluxes does follow the expected linear scaling. The results in the other DNSs are similar and are not shown here for brevity. We will revisit the issue of statistical convergence in Sec. III.

III. RESULTS

We now quantify the uncertainties in DNS statistics. The discussion focuses on high-order statistics such as skewness, kurtosis, and dissipation rate. These high-order statistics are known to be dominated by the small scales and, therefore, could also be referred to as small-scale statistics. As the DNSs differ in their discretizations in the wall-normal direction, the uncertainties are primarily a result of the wall-normal numerics and grids. Additionally, our employment of finer grids in the wall-parallel directions than the established heuristics means that the uncertainties presented in this study represent conservative estimates of the uncertainties in existing DNSs.

A. Velocity statistics

First, we quantify the uncertainties in the mean flow and the velocity root-mean-square (rms) and compare our results with these in the literature. This exercise will serve as a sanity check. Figure 4 shows the mean velocity and the rms of the streamwise velocity. The mean velocity profiles collapse. We see some differences in the streamwise velocity rms at $y^+ \approx 14$, where the profiles attain the maximum. Specifically, the SPC and SPCF results collapse well (not to say that these results can be regarded as the truth); the BS3, BS7,

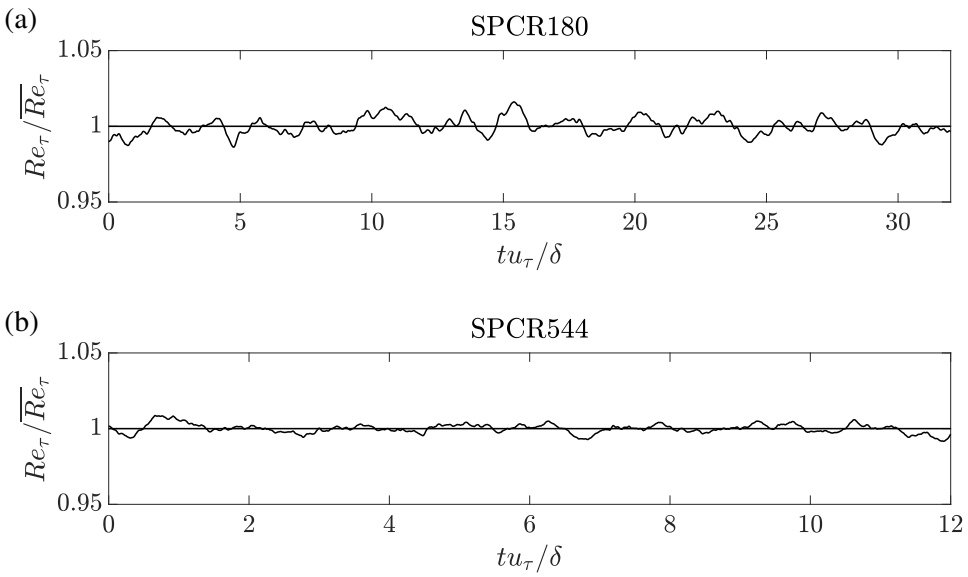

FIG. 2. A sample time history of the instantaneous friction Reynolds number for (a) SPCR180 and (b) SPCR544.

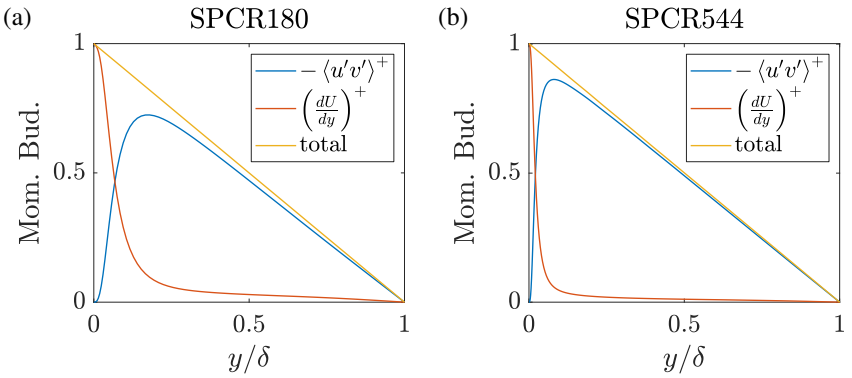

FIG. 3. The terms in the mean momentum equation. (a) SPCR180, (b) SPCR544. Here, "total" is the sum of the viscous flux and the turbulent flux. "Mom. Bud." is short for momentum budget.

and FD2 results are above the SPC and SPCF results. The peak values of the streamwise velocity rms are tabulated in Table IV. There is a 1 to 2% uncertainty, which is consistent with the result in Ref. [11, 14].

Next, we examine the high-order statistics. Figure 5 shows the skewness S

$$S = \frac{\langle u'^3 \rangle}{\langle u'^2 \rangle^{3/2}}, \tag{7}$$

and the flatness F

$$F = \frac{\langle u'^4 \rangle}{\langle u'^2 \rangle^2} \tag{8}$$

of the streamwise velocity fluctuation. Here, $\langle \cdot \rangle$ indicates the average in time and the homogeneous directions. Obtaining accurate high-order statistics is more challenging than low-order statistics [1, 21, 35], as reflected by the scattered data in figure 5. These uncertainties are significant considering that they are from "DNSs" and can all be considered as the "truth". Upon closely examining the results in figure 5, we observe that

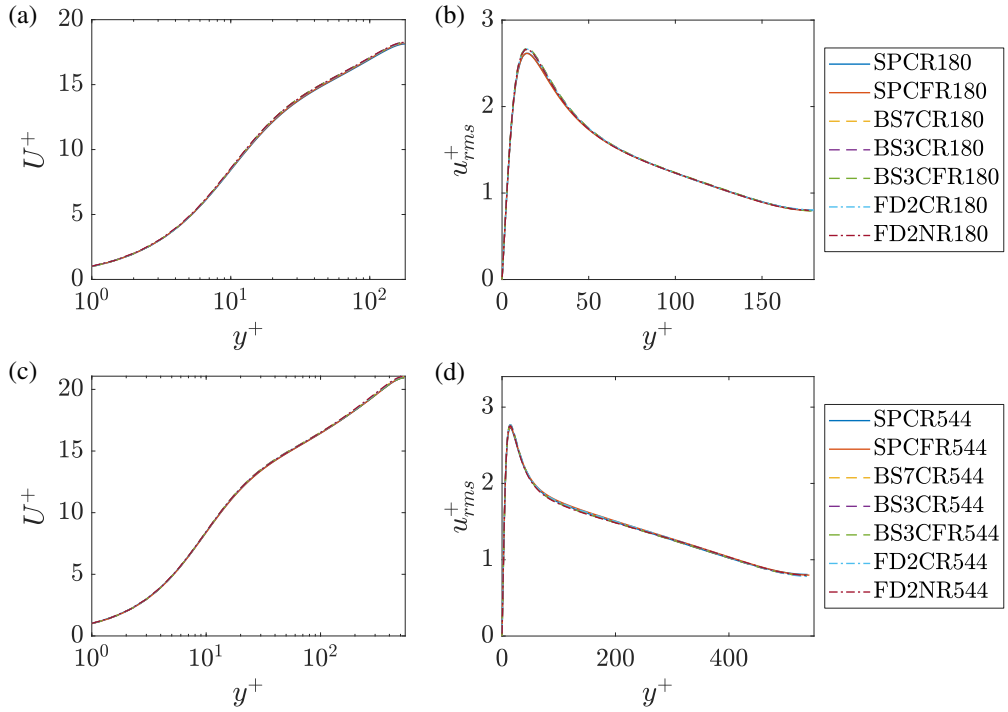

FIG. 4. Mean velocity profiles at (a) $Re_\tau = 180$ and (c) $Re_\tau = 544$. Streamwise velocity rms at (b) $Re_\tau = 180$ and (d) $Re_\tau = 544$.

TABLE IV. The peak values of the streamwise velocity rms (at $y^+ \approx 14$), the peak values of the skewness and flatness of the streamwise velocity fluctuation (at the wall), and the mean dissipation at $y^+ = 10$. We use the SPCF result as our reference. The other results are compared against the SPCF result, with + indicating a value larger and - indicating a value smaller than the SPCF result.

Re_τ	Variables	SPCF	SPC	BS7C	BS3C	BS3CF	FDC	FDN
180	$u^+_{rms,p}$	2.615	+0.000	+0.048	+0.055	+0.057	+0.050	+0.044
	S_w	0.954	-0.003	-0.014	+0.000	-0.016	-0.038	-0.062
	F_w	4.423	-0.001	-0.135	-0.134	-0.173	-0.184	-0.261
	$\langle\epsilon^+\rangle\big\vert_{y^+=10}$	0.120	-0.001	-0.004	-0.005	-0.004	-0.006	-0.010
544	$u^+_{rms,p}$	2.734	-0.006	+0.025	+0.033	+0.029	+0.034	+0.023
	S_w	1.028	+0.002	-0.016	-0.005	-0.010	-0.061	-0.096
	F_w	4.996	-0.001	-0.188	-0.197	-0.180	-0.234	-0.245
	$\langle\epsilon^+\rangle\big\vert_{y^+=10}$	0.137	+0.000	-0.002	-0.005	-0.004	-0.006	-0.009

both the skewness and the flatness arrive at the wall with a zero slope in a semi-log scale. Provided that the wall layer is well-resolved, any function that is non-singular at the wall should arrive at the wall with a zero slope because:

$$\lim_{y\to 0} \frac{dg(y)}{d\log(y)} = \lim_{y\to 0} \left(\frac{y}{\ln 10} \frac{dg(y)}{dy} \right) = 0, \tag{9}$$

where g is a generic function. Equation (9) serves as a sanity check, and the results in Fig. 5 pass this sanity check. Furthermore, SPC and SPCF predict skewness and flatness that are larger than the other DNSs at the wall. Table IV tabulates the skewness and flatness at the wall. Comparing the SPCR, BS7CR, BS3CR, and FD2CR results, we see that the numerics is responsible for a 5% uncertainty in the skewness statistics and a 7% uncertainty in the flatness statistics. Comparing FD2CR and FD2NR, we see that stretching the

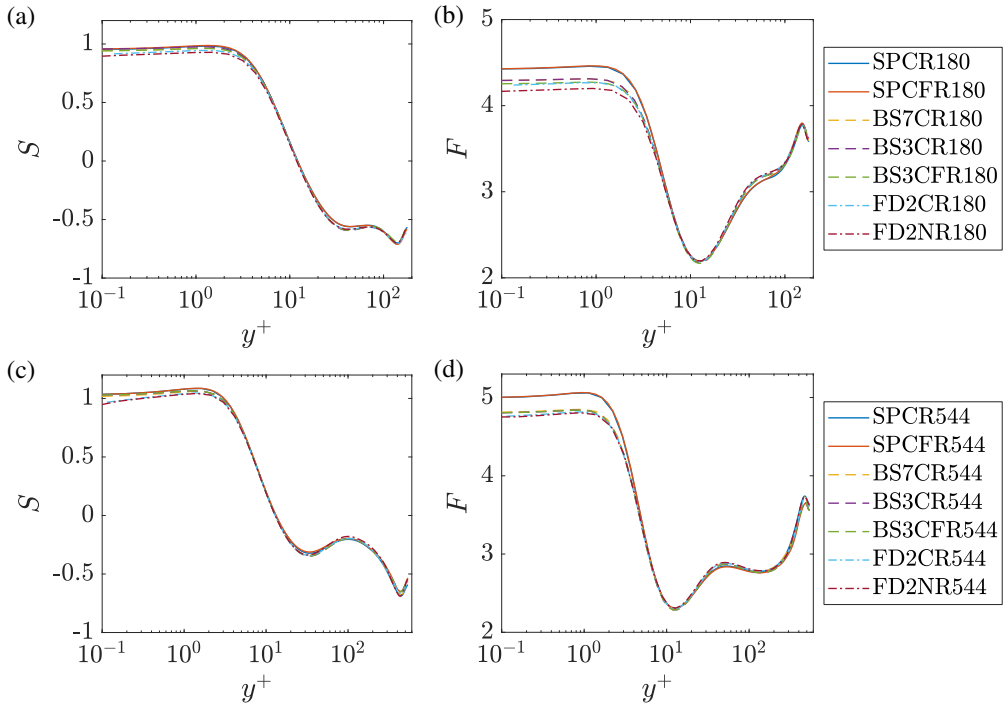

FIG. 5. Skewness of the streamwise velocity fluctuation at (a) $Re_\tau = 180$ and (c) $Re_\tau = 544$. Flatness of the streamwise velocity fluctuation at (b) $Re_\tau = 180$ and (d) $Re_\tau = 544$.

grid according to a cosine function or the natural stretching function leads to 3% and 4% uncertainty in the skewness and 2% and 0.2% uncertainty in the flatness for R180 and R544 cases, respectively. Finally, comparing the BSCR180 and BSCFR180 results or the BSCR544 and BSCFR544 results, there is a 1% uncertainty. These results suggest that the DNSs are not grid-converged. This is not very surprising. A commonly quoted criterion for solutions free from artificial numerical oscillations is $Pe_\Delta \leq 2$, where $Pe_\Delta = \Delta U/\nu$ is the cell Peclet number. In these DNSs, Pe_Δ is between 0 to about 200. Consequently, the solutions are not free from numerical oscillations and therefore are far from grid converged. Again, we only quantify the uncertainty in the statistics and make no judgment about the numerics or the grid stretching strategies.

B. Dissipation

We quantify the uncertainties in dissipation. The viscous dissipation ϵ is defined as follows

$$\epsilon = \nu \left\langle \frac{\partial u_i'}{\partial x_j} \frac{\partial u_i'}{\partial x_j} \right\rangle, \tag{10}$$

where the summation of repeated indices is implied. The present discussion focuses on the viscous sublayer and the buffer layer. Aside from the fact that the flow is highly intermittent and therefore difficult to resolve in the wall layer, the buffer layer is dynamically important as the topology of eddies changes from sheet-like near the wall to rod-like away from the wall there [36].

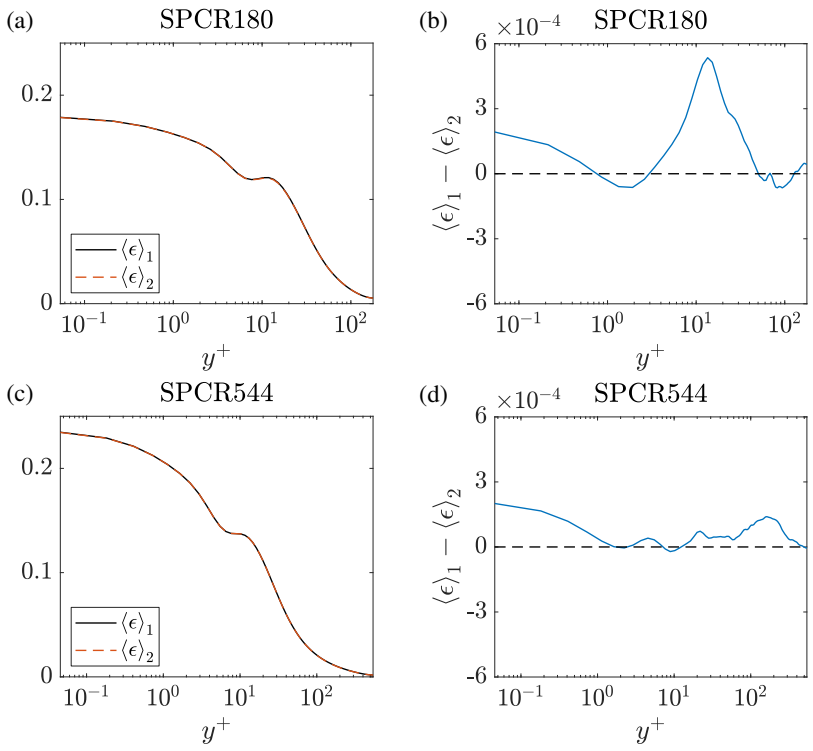

FIG. 6. Mean dissipation in (a) SPCR180, and (c) SPCR544. Here, $\langle\epsilon\rangle_1$ is the average over a time period of T_r, and $\langle\epsilon\rangle_2$ is the average over a time period of $2T_r$. (b, d) The difference between $\langle\epsilon\rangle_1$ and $\langle\epsilon\rangle_2$.

1. *Low Reynolds numbers*

We revisit the issue of statistical convergence. To assess the statistical convergence of our dissipation statistics, we compare statistics averaged over T_r and $2T_r$ for SPCR180 and SPCR544, respectively. The two statistics are referred to as $\cdot_1$ and $\cdot_2$. Here, T_r is the averaging time listed in Table II. We can claim statistical convergence if the two statistics averaged over a period of T_r and $2T_r$ are similar. Figure 6 (a, c) shows the computed mean dissipation $\langle\epsilon\rangle_1$ and $\langle\epsilon\rangle_2$ and figure 6 (b, d) show the difference between $\langle\epsilon\rangle_1$ and $\langle\epsilon\rangle_2$. The convergence error is less than 0.5% of the maximum dissipation. Figure 7 show the computed probability density function $P(\epsilon)$ at three y^+ locations, i.e., $y^+ = 0$, 10 and 30. Integrating the PDF from $\epsilon^+ = 0$ to the three gray vertical lines in the figure gives 90%, 99%, and 99.9%. Figure 7 shows that there is barely any difference between P_1 and P_2.

Next, we quantify the uncertainties in the dissipation data. Figures 8 (a, c) show the viscous dissipation in all DNSs. We take the SPCF result as our reference. Here, the SPCF result is taken as the reference, not the truth. Again, we take a user's perspective and make no judgment about the numerics or grid distribution Figures 8 (b, d) show the difference between the other DNSs and SPCF. We observe the following. The SPC and SPCF results collapse; the BS3C and BS3CF results also collapse reasonably well. The values of the dissipation at $y^+ = 10$ are tabulated in Table IV, and there is a 7% uncertainty. Upon closely examining the results, we see that the FD results are further away from the SP results than the BS results; among BS3 and BS7, the BS7 results are closer to the SP results than the BS3 results; among FD2N and FD2C, the FD2C results are closer to the SP results than the FD2N results.

Figure 9 shows the PDF of the viscous dissipation at $y^+ = 0$, 10, and 30 in all DNSs. The BS, FD, and SP results differ. The difference is most noticeable at large ϵ values, which is physical since a significant instantaneous dissipation gives rise to a small instantaneous Kolmogorov length scale and is hard to resolve [19, 20, 37]. Integrating the PDFs in the plots to the three vertical lines approximately gives 0.9, 0.99, and

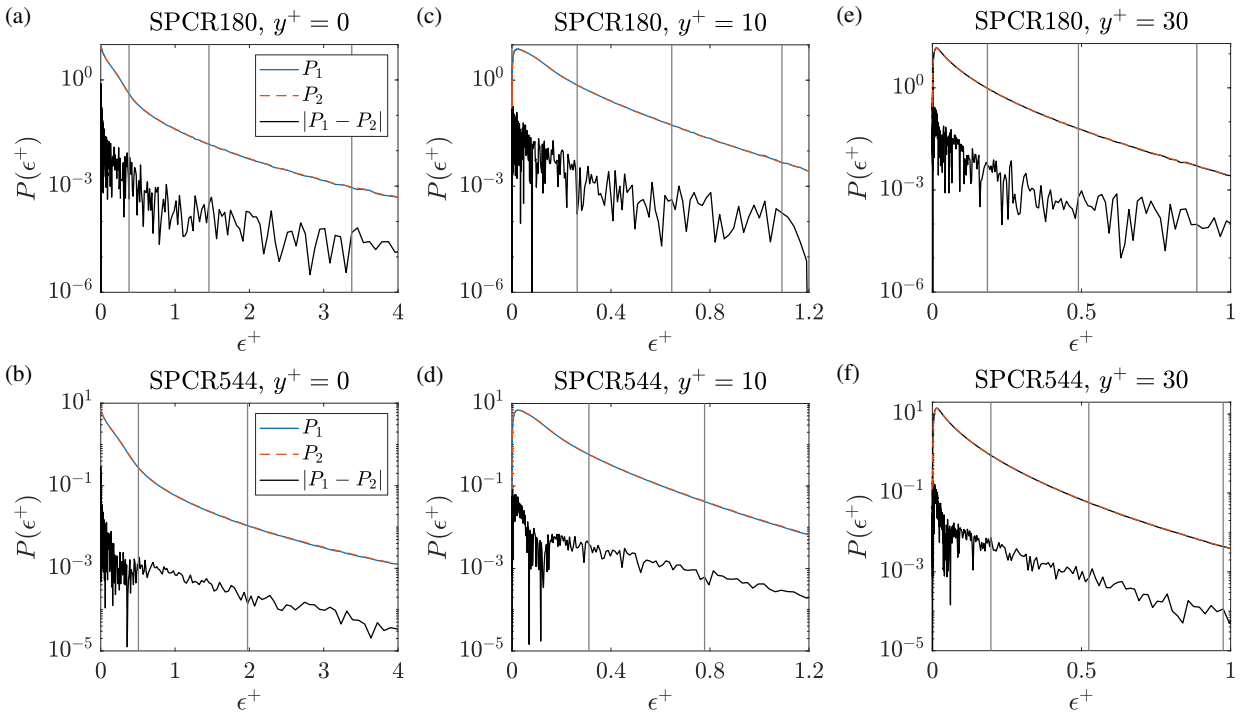

FIG. 7. Probability density function (PDF) of the instantaneous viscous dissipation at (a, b) $y^+ = 0$, (c, d) $y^+ = 10$, (e, f) $y^+ = 30$. (a, c, e) $Re_\tau = 180$, (b, d, f) $Re_\tau = 544$. Integrating the PDF from $\epsilon^+ = 0$ to the three vertical lines gives 90%, 99%, and 99.9%.

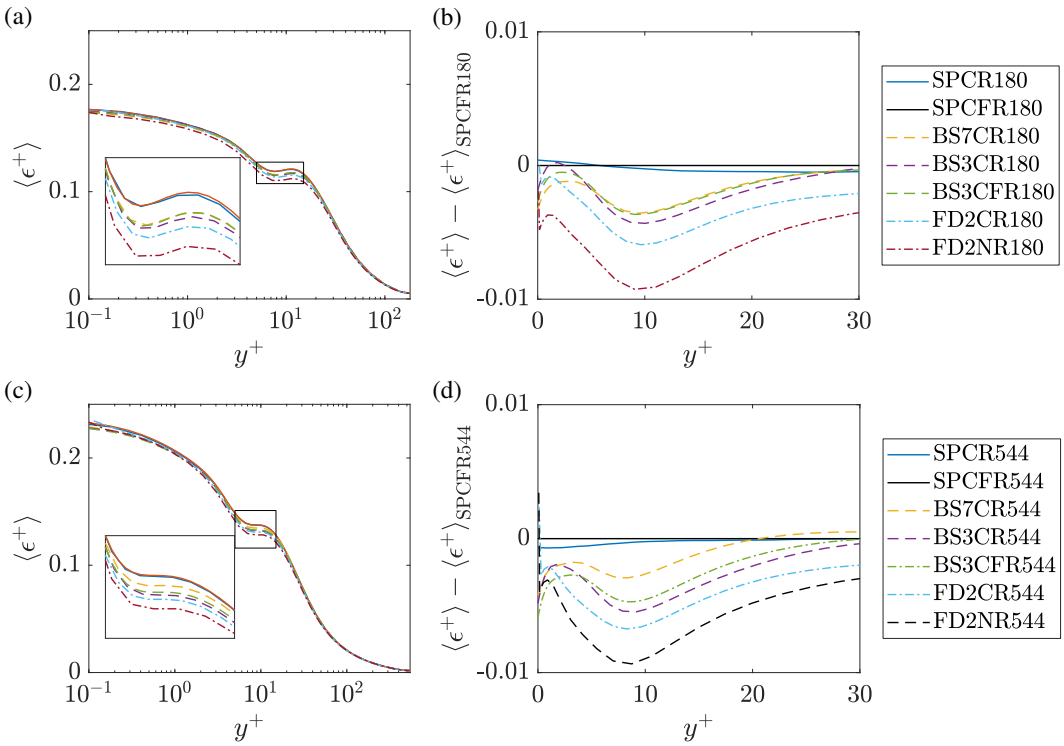

FIG. 8. Mean dissipation in (a) the $Re_\tau = 180$ cases and (c) the $Re_\tau = 544$ cases. The difference between the other cases and the SPCF cases at (b) the $Re_\tau = 180$ cases and (d) the $Re_\tau = 544$. The solid black lines in (b, d) are at 0.

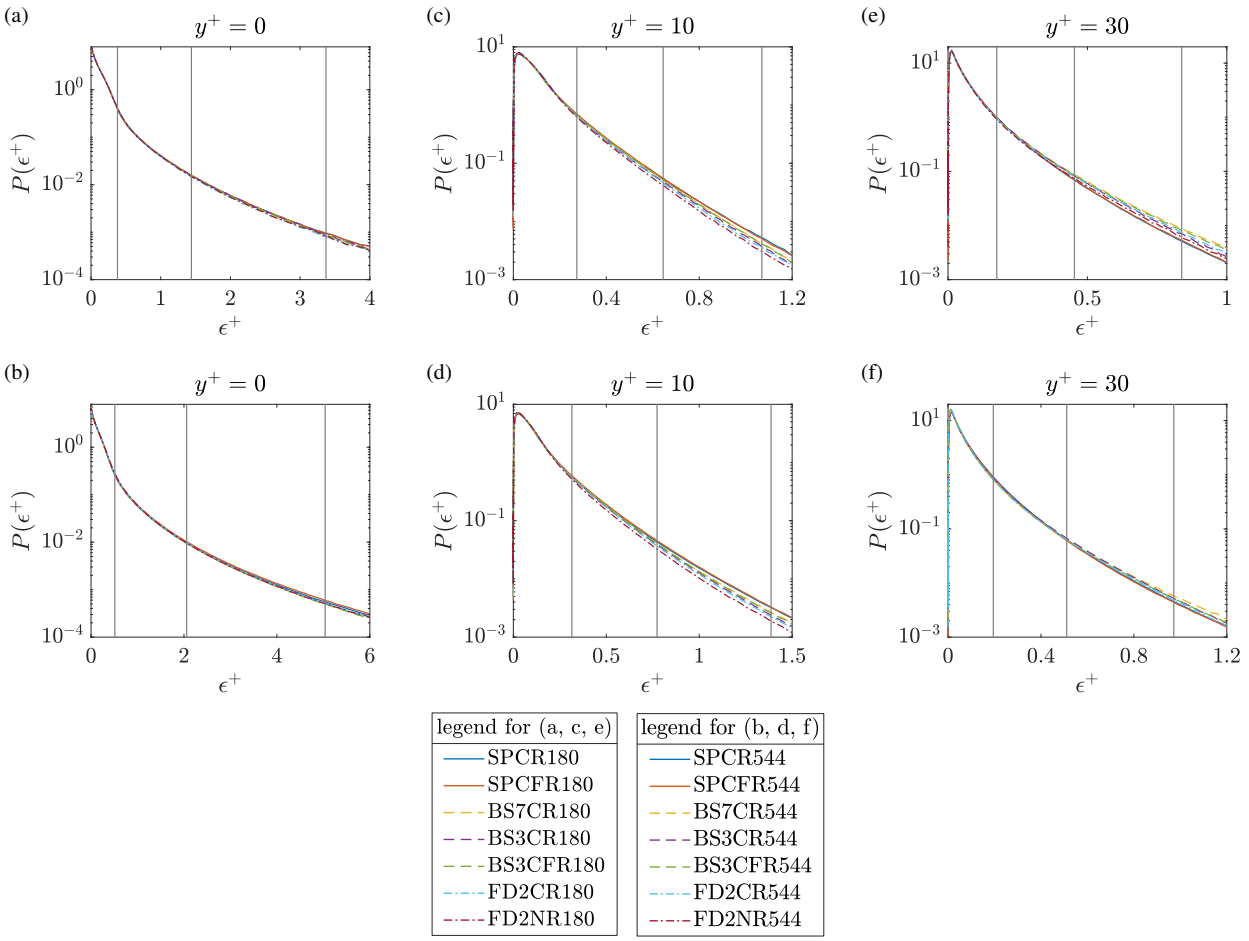

FIG. 9. PDF of the viscous dissipation in our DNSs. Integrating the PDF from 0 to the three gray vertical lines gives 90%, 99%, and 99.9%.

0.999. If we keep one significant digit, there are about 0.1%, 10%, and 1% events that show uncertainty at $y^+ = 10$, $y^+ = 0$, and 30, respectively, since the PDFs begin to show uncertainty at the third, the first, and the second vertical lines in (b, d, f).

To summarize, different wall-normal grids and numerics, while all are conforming to the established heuristics, lead to a 7% uncertainty in the computed mean dissipation rate at $Re_\tau = 180$ and 550. About 99.9%, 90%, and 99% of the instantaneous dissipation events are resolved at $y^+ = 0$, 10, and 30 at $Re_\tau = 180$ and 544.

2. High Reynolds numbers

Assessing the uncertainties in DNS statistics at high Reynolds numbers is not straightforward because of DNSs' high cost at high Reynolds numbers. Nonetheless, relying on Reynolds number scalings and data at a low Reynolds number, it is possible to estimate the uncertainties at high Reynolds numbers without additional calculations.

The estimate relies on the following two hypotheses. First, given a code and the grid resolution in wall units, an instantaneous dissipation event that is well-resolved at one Reynolds number remains well-resolved at another Reynolds number. Second, the probability density function of $\epsilon^+ / \langle \epsilon^+ \rangle$ at a given y^+ in the constant stress layer is independent of the Reynolds number and is universal. The first hypothesis should

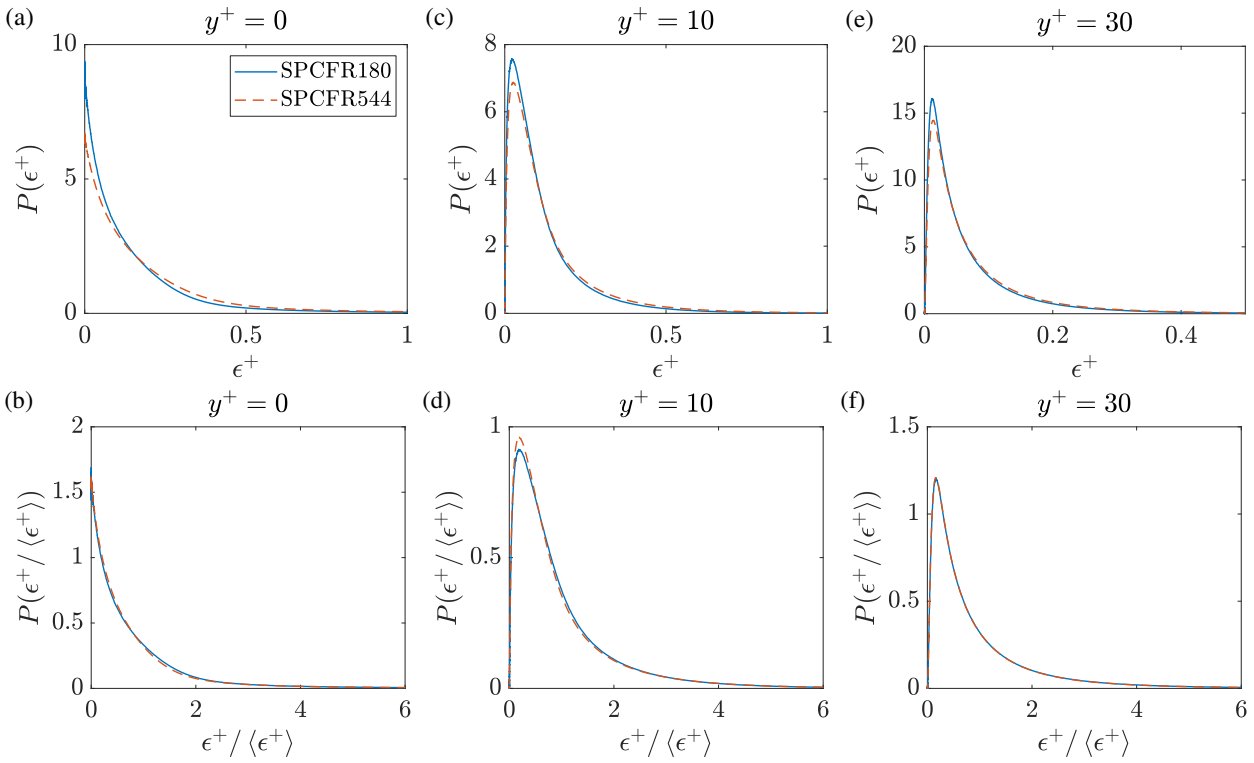

FIG. 10. PDFs of ϵ^+ at (a) $y^+ = 0$, (c) $y^+ = 10$, and (e) $y^+ = 30$. PDFs of $\epsilon^+/\langle\epsilon^+\rangle$ at (b) $y^+ = 0$, (d) $y^+ = 10$, and (f) $y^+ = 30$.

need no further explanation. The second hypothesis has received some empirical support [38]. Figure 10 show $P(\epsilon^+/\langle\epsilon^+\rangle)$ and $P(\epsilon^+)$ at $y^+ = 0$, 10, and 30, and we see that $P(\epsilon^+/\langle\epsilon^+\rangle)$ does collapse for small epsilon values. Large ϵ values correspond to rare events, which are not our concern in this paper.

The mean dissipation $\langle\epsilon\rangle$ in $P(\epsilon/\langle\epsilon\rangle)$ is unknown. Here, we follow [39] and assume that $\langle\epsilon^+\rangle/\langle\epsilon_w^+\rangle$ is a universal function of $y^+\langle\epsilon_w^+\rangle$, i.e.,

$$\langle\epsilon^+\rangle/\langle\epsilon_w^+\rangle = g(y^+\langle\epsilon_w^+\rangle), \tag{11}$$

where g is a generic universal function and can be obtained at a low Reynolds number. With Eq. (11), if we know the Reynolds number scaling of $\langle\epsilon_w^+\rangle$, we would know $\langle\epsilon\rangle$ at all y^+ and Reynolds numbers. The Reynolds number scaling of $\langle\epsilon_w^+\rangle$ is still a research topic. Chen et al. [6] argued that

$$\langle\epsilon_w^+\rangle = \langle\epsilon_{x,w}^+\rangle + \langle\epsilon_{z,w}^+\rangle = a_1 - b_1 Re_\tau^{-1/4}, \tag{12}$$

where $a_1 = 0.38$, $b_1 = 0.73$. Yang and Lozano-Duran [4] argued that

$$\langle\epsilon_w^+\rangle = a_2 + b_2\ln(Re_\tau). \tag{13}$$

where $a_2 = 0.0166$, $b_2 = 0.0329$. Schlatter and Orlu [8] and Diaz et al. [9] argued that

$$\langle\epsilon_w^+\rangle = [a_3 + b_3\ln(Re_\tau)]^2, \tag{14}$$

where $a_3 = 0.2562$, $b_3 = 0.0342$. The coefficients are the best fits of the available data [27].

The information above allows us to infer the uncertainty in a high Reynolds number DNS using data at a low Reynolds number. The steps are as follows. Consider a DNS where events $\epsilon^+ < \epsilon_{\rm lim}^+$ are resolved but events $\epsilon^+ > \epsilon_{\rm lim}^+$ are not. This DNS resolves $\mathcal{P}\times 100\%$ dissipation events, where $\mathcal{P}$ is

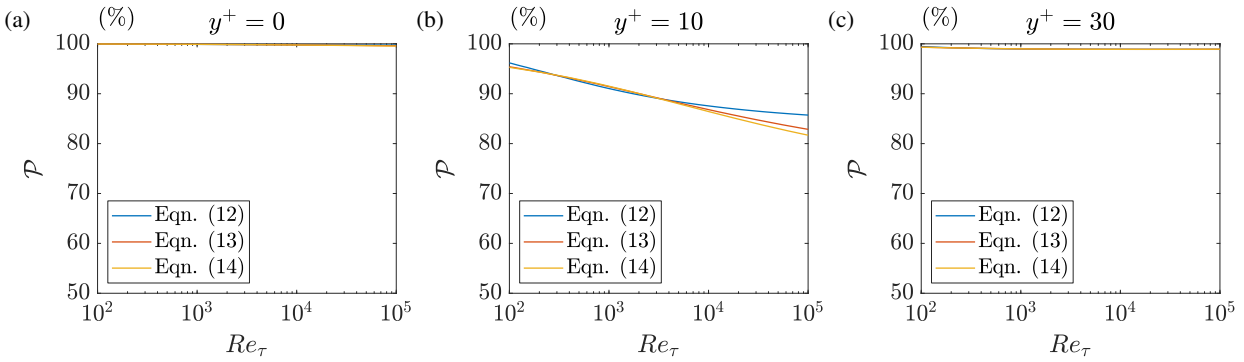

FIG. 11. The proportion of dissipation events well-resolved in DNSs. (a) $y^+ = 0$, (b) $y^+ = 10$, (c) $y^+ = 30$. Blue solid line: assuming the wall dissipation scales as Eq. (12); red dash line: assuming the wall dissipation scales as Eq. (13); yellow dash-dot line: assuming the wall dissipation scales as Eq. (14).

$$\mathcal{P}(y^+, Re_\tau) = \int_0^{\epsilon^+_{\rm lim}} P(\epsilon^+; y^+, Re_\tau) d\epsilon^+. \tag{15}$$

Here, $P(\epsilon^+; y^+, Re_\tau)$ is the probability density function of ϵ^+, and the cumulative density function $\mathcal{P}$ is a function of both y^+ and Re_τ. According to the second hypothesis, the PDF of $\epsilon^+ / \langle \epsilon^+ \rangle$ is a function of y^+ only, and therefore

$$P(\epsilon^+; y^+, Re_\tau) d\epsilon^+ = P(\epsilon^+ / \langle \epsilon^+ \rangle ; y^+) d\left(\epsilon^+ / \langle \epsilon^+ \rangle\right), \tag{16}$$

where $P(\epsilon^+ / \langle \epsilon^+ \rangle ; y^+)$ is the probability density function of $\epsilon^+ / \langle \epsilon^+ \rangle$ and can be measured in a low Reynolds number DNS, e.g., from figure 10. Furthermore, because of Eq. (11), we can re-write Eq. (16) as

$$P(\epsilon^+; y^+, Re_\tau) d\epsilon^+ = P\left(\frac{\epsilon^+}{g(\langle \epsilon_w^+ \rangle y^+) \epsilon_w^+}; y^+ \right) d\epsilon^+ \Big/ \left(g(\langle \epsilon_w^+ \rangle y^+) \epsilon_w^+ \right). \tag{17}$$

It then follows from Eqs. (15) and (17) that

$$\mathcal{P}(y^+, Re_\tau) = \int_0^{\epsilon^+_{\rm lim}} P\left(\frac{\epsilon^+}{g(\langle \epsilon_w^+ \rangle y^+) \epsilon_w^+}; y^+ \right) \frac{d\epsilon^+}{g(\langle \epsilon_w^+ \rangle y^+) \epsilon_w^+}, \tag{18}$$

which, when given $\epsilon^+_{\rm lim}$, can be readily evaluated for an arbitrary Re_τ and y^+.

The results in figure 9 suggests that $\epsilon^+_{\rm lim} = 5.04$, 0.31, and 0.51 for $y^+ = 0$, 10, and 30. We substitute these numbers in Eq. (18) and compute $\mathcal{P}$ as a function of Re_τ for $y^+ = 0$, 10, and 30. Figure 11 shows the results. Different Reynolds number scalings of the wall dissipation give slightly different estimates. However, the trend is the same: if similar wall-normal grid resolutions are used at low and high Reynolds numbers, the DNS will resolve fewer dissipation events at high Reynolds numbers. More specifically, if we were to use a similar wall-normal grid, i.e., $\Delta y_w^+ = 0.05$, $\Delta y_c = 1.5\eta$, naturally or cosine stretched, for a channel flow DNS at $Re_\tau = 10^5$, we would be resolving about 99.8%, 86.4%∼87.6%, and 98.9% events at $y^+ = 0$, 10, and 30, respectively.

IV. CONCLUSIONS

We take the perspective of someone who uses DNS data and quantify the uncertainty in the DNS-computed statistics. By limiting the uncertainty due to a finite sampling time and by employing the same numerics and grids in the wall-parallel directions, we show that the wall-normal numerics and grids contribute to (at least) 6%, 6%, and 7% uncertainty in the skewness, kurtosis, and mean viscous dissipation at low Reynolds numbers

($Re_\tau = 544$). The impact of numerics is found to be more significant than that of the grid distribution. Since we used longer averaging times and finer grids in the wall-parallel directions than those in previous literature, the results here suggest that existing data may have larger uncertainties in these statistics. Furthermore, because turbulence is more intermittent at higher Reynolds numbers, a given grid resolution (in terms of wall units) resolves fewer instantaneous dissipation events at higher Reynolds numbers. Our analysis indicates that the established heuristics for grid resolution resolves about 90% and 87% of the instantaneous dissipation events at $Re_\tau = 544$ and 10^5, respectively.

In contrast to previous studies that focused on the mean velocity and velocity rms, we demonstrate that while DNS-computed low-order statistics are highly accurate, higher-order statistics have a higher level of uncertainty. Last, we note that we made no judgment about the discretization methods or the grids. A more in-depth investigation would be needed to determine the "best" numerical strategy for channel flow DNS—if there is a "best" strategy.

ACKNOWLEDGEMENT

The authors thank MK Lee for the fruitful discussion and constructive comments. XY acknowledges NSF Award Number 2231037. YS acknowledges the financial support from NSFC 91752202.

[1] J. Kim, P. Moin, and R. Moser, "Turbulence statistics in fully developed channel flow at low Reynolds number," *J. Fluid Mech.*, vol. 177, pp. 133–166, 1987.

[2] S. Hoyas and M. Oberlack, "Wall turbulence at $Re_\tau = 10k$: Kinematics and symmetry scaling laws," *Bulletin of the American Physical Society*, 2022.

[3] P. Moin and K. Mahesh, "Direct numerical simulation: a tool in turbulence research," *Annu. Rev. Fluid Mech.*, vol. 30, no. 1, pp. 539–578, 1998.

[4] X. I. Yang and A. Lozano-Durán, "A multifractal model for the momentum transfer process in wall-bounded flows," *J. Fluid Mech.*, vol. 824, 2017.

[5] X. Chen and K. R. Sreenivasan, "Reynolds number scaling of the peak turbulence intensity in wall flows," *J. Fluid Mech.*, vol. 908, 2021.

[6] X. Chen and K. R. Sreenivasan, "Law of bounded dissipation and its consequences in turbulent wall flows," *J. Fluid Mech.*, vol. 933, 2022.

[7] P. E. Chen, Y. Lv, H. H. Xu, Y. Shi, and X. I. Yang, "LES wall modeling for heat transfer at high speeds," *Phys. Rev. Fluids*, vol. 7, no. 1, p. 014608, 2022.

[8] P. Schlatter and R. Örlü, "Assessment of direct numerical simulation data of turbulent boundary layers," *J. Fluid Mech.*, vol. 659, pp. 116–126, 2010.

[9] C. Diaz-Daniel, S. Laizet, and J. C. Vassilicos, "Wall shear stress fluctuations: Mixed scaling and their effects on velocity fluctuations in a turbulent boundary layer," *Phys. Fluids*, vol. 29, no. 5, p. 055102, 2017.

[10] T. A. Oliver, N. Malaya, R. Ulerich, and R. D. Moser, "Estimating uncertainties in statistics computed from direct numerical simulation," *Phys. Fluids*, vol. 26, no. 3, p. 035101, 2014.

[11] A. Vreman and J. G. Kuerten, "Comparison of direct numerical simulation databases of turbulent channel flow at Re_τ= 180," *Phys. Fluids*, vol. 26, no. 1, p. 015102, 2014.

[12] E. Jeyapaul, G. N. Coleman, and C. L. Rumsey, "Higher-order and length-scale statistics from DNS of a decelerated planar wall-bounded turbulent flow," *Int. J. Heat Fluid Flow*, vol. 54, pp. 14–27, 2015.

[13] R. L. Thompson, L. E. B. Sampaio, F. A. de Bragança Alves, L. Thais, and G. Mompean, "A methodology to evaluate statistical errors in DNS data of plane channel flows," *Comput. Fluids*, vol. 130, pp. 1–7, 2016.

[14] M. Bernardini, S. Pirozzoli, and P. Orlandi, "Velocity statistics in turbulent channel flow up to $Re_\tau = 4000$," *J. Fluid Mech.*, vol. 742, pp. 171–191, 2014.

[15] H. Choi and P. Moin, "Grid-point requirements for large eddy simulation: Chapman's estimates revisited," *Phys. Fluids*, vol. 24, no. 1, p. 011702, 2012.

[16] X. I. Yang and K. P. Griffin, "Grid-point and time-step requirements for direct numerical simulation and large-eddy simulation," *Phys. Fluids*, vol. 33, no. 1, p. 015108, 2021.

[17] S. Pirozzoli and P. Orlandi, "Natural grid stretching for DNS of wall-bounded flows," *J. Comput. Phys.*, vol. 439, p. 110408, 2021.

[18] S. Pirozzoli, M. Bernardini, and P. Orlandi, "Passive scalars in turbulent channel flow at high Reynolds number," *J. Fluid Mech.*, vol. 788, pp. 614–639, 2016.

[19] D. Donzis, P. Yeung, and K. Sreenivasan, "Dissipation and enstrophy in isotropic turbulence: resolution effects and scaling in direct numerical simulations," *Phys. Fluids*, vol. 20, no. 4, p. 045108, 2008.

[20] V. Yakhot and K. R. Sreenivasan, "Anomalous scaling of structure functions and dynamic constraints on turbulence simulations," *J. Stat. Phys.*, vol. 121, no. 5, pp. 823–841, 2005.

[21] X. I. Yang, J. Hong, M. Lee, and X. L. Huang, "Grid resolution requirement for resolving rare and high intensity wall-shear stress events in direct numerical simulations," *Phys. Rev. Fluids*, vol. 6, no. 5, p. 054603, 2021.

[22] R. D. Moser, J. Kim, and N. N. Mansour, "Direct numerical simulation of turbulent channel flow up to Re_τ= 590," *Phys. Fluids*, vol. 11, no. 4, pp. 943–945, 1999.

[23] J. C. Del Alamo, J. Jiménez, P. Zandonade, and R. D. Moser, "Scaling of the energy spectra of turbulent channels," *J. Fluid Mech.*, vol. 500, pp. 135–144, 2004.

[24] A. Lozano-Durán and J. Jiménez, "Effect of the computational domain on direct simulations of turbulent channels up to Re_τ= 4200," *Phys. Fluids*, vol. 26, no. 1, p. 011702, 2014.

[25] Y. Yamamoto and Y. Tsuji, "Numerical evidence of logarithmic regions in channel flow at Re_τ= 8000," *Phys. Rev. Fluids*, vol. 3, no. 1, p. 012602, 2018.

[26] H. Abe, H. Kawamura, and Y. Matsuo, "Surface heat-flux fluctuations in a turbulent channel flow up to Re_τ= 1020 with Pr= 0.025 and 0.71," *Int. J. Heat Fluid Flow*, vol. 25, no. 3, pp. 404–419, 2004.

[27] M. Lee and R. D. Moser, "Direct numerical simulation of turbulent channel flow up to $Re_\tau \approx 5200$," *J. Fluid Mech.*, vol. 774, pp. 395–415, 2015.

[28] J. Graham, K. Kanov, X. Yang, M. Lee, N. Malaya, C. Lalescu, R. Burns, G. Eyink, A. Szalay, R. Moser, *et al.*, "A web services accessible database of turbulent channel flow and its use for testing a new integral wall model for LES," *J. Turbul.*, vol. 17, no. 2, pp. 181–215, 2016.

[29] E. Bou-Zeid, C. Meneveau, and M. Parlange, "A scale-dependent lagrangian dynamic model for large eddy simulation of complex turbulent flows," *Phys. Fluids*, vol. 17, no. 2, p. 025105, 2005.

[30] S. Altland, X. Zhu, S. McClain, R. Kunz, and X. Yang, "Flow in additively manufactured super-rough channels," *Flow*, vol. 2, p. E19, 2022.

[31] W. Zhang, X. Zhu, X. I. Yang, and M. Wan, "Evidence for Raupach et al.'s mixing-layer analogy in deep homogeneous urban-canopy flows," *J. Fluid Mech.*, vol. 944, 2022.

[32] H. H. Xu, S. J. Altland, X. I. Yang, and R. F. Kunz, "Flow over closely packed cubical roughness," *J. Fluid Mech.*, vol. 920, 2021.

[33] P. Forooghi, X. I. Yang, and M. Abkar, "Roughness-induced secondary flows in stably stratified turbulent boundary layers," *Phys. Fluids*, vol. 32, no. 10, p. 105118, 2020.

[34] S. Hoyas and J. Jiménez, "Scaling of the velocity fluctuations in turbulent channels up to Re_τ= 2003," *Phys. Fluids*, vol. 18, no. 1, p. 011702, 2006.

[35] X. I. Yang, I. Marusic, and C. Meneveau, "Moment generating functions and scaling laws in the inertial layer of turbulent wall-bounded flows," *J. Fluid Mech.*, vol. 791, 2016.

[36] P. Orlandi, "The importance of wall-normal Reynolds stress in turbulent rough channel flows," *Phys. Fluids*, vol. 25, no. 11, p. 110813, 2013.

[37] P. Yeung, K. Sreenivasan, and S. Pope, "Effects of finite spatial and temporal resolution in direct numerical simulations of incompressible isotropic turbulence," *Phys. Rev. Fluids*, vol. 3, no. 6, p. 064603, 2018.

[38] P. E. Hamlington, D. Krasnov, T. Boeck, and J. Schumacher, "Local dissipation scales and energy dissipation-rate moments in channel flow," *J. Fluid Mech.*, vol. 701, pp. 419–429, 2012.

[39] T. Wei, "Scaling of turbulent kinetic energy and dissipation in turbulent wall-bounded flows," *Phys. Rev. Fluids*, vol. 5, no. 9, p. 094602, 2020.